J Geod (2015) 89:427–445
DOI 10.1007/s00190-015-0788-2

ORIGINAL ARTICLE

# Timing group delay and differential code bias corrections for BeiDou positioning

**Fei Guo · Xiaohong Zhang · Jinling Wang**

Received: 26 August 2014 / Accepted: 31 December 2014 / Published online: 13 January 2015


**Abstract** This article first clearly figures out the relationship between parameters of timing group delay (TGD) and differential code bias (DCB) for BDS, and demonstrates the equivalence of TGD and DCB correction models combining theory with practice. The TGD/DCB correction models have been extended to various occasions for BDS positioning, and such models have been evaluated by real triple-frequency datasets. To test the effectiveness of broadcast TGDs in the navigation message and DCBs provided by the Multi-GNSS Experiment (MGEX), both standard point positioning (SPP) and precise point positioning (PPP) tests are carried out for BDS signals with different schemes. Furthermore, the influence of differential code biases on BDS positioning estimates such as coordinates, receiver clock biases, tropospheric delays and carrier phase ambiguities is investigated comprehensively. Comparative analysis show that the unmodeled differential code biases degrade the performance of BDS SPP by a factor of two or more, whereas the estimates of PPP are subject to varying degrees of influences. For SPP, the accuracy of dual-frequency combinations is slightly worse than that of single-frequency, and they are much more sensitive to the differential code biases, particularly for the B2B3 combination. For PPP, the uncorrected differential code biases are mostly absorbed into the receiver clock bias and carrier phase ambiguities and thus resulting in a much longer convergence time. Even though the influence of the differential code biases could be mitigated over time and comparable positioning accuracy could be achieved after convergence, it is suggested to properly handle with the differential code biases since it is vital for PPP convergence and integer ambiguity resolution.

**Keywords** BeiDou navigation satellite system (BDS) · Timing group delay (TGD) · Differential code bias (DCB) · Correction model · Precise point positioning (PPP) · Standard point positioning (SPP)

## 1 Introduction

Following the great success of the global positioning system (GPS) and the completion of the Russian GLONASS system, BeiDou navigation satellite system (BDS) is the third navigation satellite system that offers an independent regional service now and global positioning service by 2020. The current BDS constellation comprises a total of 14 active satellites: 5 geostationary satellites (GEO), 5 satellites in inclined geosynchronous orbit (IGSO) and 4 satellites in medium altitude earth orbits (MEO). Given the placement of the GEO and IGSO satellites, the BDS provides best coverage in the Asia-Pacific region. Users in this region can benefit from BDS as either an individual system or as a supplement to the currently used systems such as GPS and GLONASS (Montenbruck et al. 2013; Shi et al. 2013; Yang et al. 2014).

GNSS (e.g., GPS, GLONASS, and BDS) pseudoranges are well known to be affected by instrumental biases (Rao 2007; Li et al. 2014). To cope with this problem, timing group delay (TGD) or differential code bias (DCB) parameters are commonly used for pseudorange corrections at the user ends. For the legacy GPS and GLONASS, it has been a common practice to define clock offsets in both broadcast and precise ephemeris products with respect to an ionosphere-free dual-

F. Guo · X. Zhang (✉)
School of Geodesy and Geomatics, Wuhan University,
129 Luoyu Road, Wuhan 430079, China
e-mail: xhzhang@sgg.whu.edu.cn

F. Guo · J. Wang
School of Civil and Environment Engineering, University of New Southwales, Sydney, NSW 2052, Australia

frequency combination of conventional reference signals [L1/L2 P(Y)-code] (Montenbruck and Steigenberger 2013). GPS/GLONASS applications using other signals or combined signals differing from the conventional reference signal should apply TGD or DCB corrections, which are essential for pseudorange-based positioning, timing and ionosphere modeling (Wu et al. 2013; Montenbruck et al. 2014). Parameters designated as timing group delay (TGD) and inter-signal corrections (ISC) in the navigation message are commonly used to compensate the differential code biases in real time for single-frequency users. Correction terms such as, TGD, $ISC_{L1C/A}$ and $ISC_{L2C}$, are initially defined to account for the effect of space vehicle (SV) group delay differential between L1 P(Y) and L2 P(Y), L1 P(Y) and L1 C/A, and between L1 P(Y) and L2 C, respectively (Tetewsky et al. 2009). In addition, more accurate differential code bias parameters designated as DCBs (such as $DCB_{P1P2}$, $DCB_{P1C1}$ and $DCB_{P2C2}$) are provided by GNSS communities to account for the same delay as TGD and ISCs, particularly for the post-processing applications (Schaer and Steigenberger 2006; Schaer 2008, 2012). The broadcast TGD values are referenced to an empirical absolute instrumental (satellite) bias, whereas DCB values are in a relative sense to reflect the differential hardware (the satellite or receiver) delay between two different code observations obtained on the same or two different frequencies (Li et al. 2012).

The values of TGD, ISCs and DCBs are routinely determined for the legacy GPS and GLONASS signals but only limited knowledge of the TGD and DCB is presently available for the new BDS. As the only one truly operating triple-frequency navigation system, all BDS satellites transmit B1, B2 and B3 signals, thus having more TGD and DCB parameters, in addition to the increased number of combinations. Moreover, the clock reference chosen by BDS is in a different manner rather than for other GNSS constellations. According to the BDS Interface Control Document (ICD, see http://www.beidou.gov.cn), currently BDS adopts the single-frequency B3 signal as the primary clock reference in broadcast ephemeris, while the precise ephemeris (and clock) products refer to the B1/B2 ionosphere-free dual-frequency observable (He et al. 2013; Zhao et al. 2013; Deng et al. 2014; Lou et al. 2014). Therefore, the TGD/DCB corrections of BDS are not exactly the same as that of GPS or GLONASS. Even though a correction model for BDS is given in Montenbruck and Steigenberger (2013), it is only applicable to standard point positioning. Such correction models should be further extended to cover all situations. In addition, the effectiveness of broadcast TGDs and DCBs as well as their influences on positioning are presently not clear due to the lack of comprehensive analysis in current literature.

Within this paper, we first provide a summary of the current available TGD and DCB parameters for BDS, and describe their relationship combining theory with practice. Thereafter the TGD or DCB correction models are developed to cover all critical BDS positioning scenarios. Furthermore, comprehensive analysis of the influence of differential code biases on standard point positioning (SPP) and precise point positioning (PPP) has been performed using triple-frequency BDS data.

## 2 Current status of BDS TGDs/DCBs

With the release of a public ICD, BDS information such as system, signal, and navigation messages is now available for real-time users. TGDs are usually broadcasted through navigation message for real-time applications, while the DCBs are precisely estimated by GNSS communities and provided for the precise post-processing users. The broadcast satellite TGDs, also known as "SV group delay differential" are initially determined from the pre-launching calibration data. To reflect the actual on-orbit group delay differential and fit well with the DCBs estimated by some IGS organizations, the TGDs are subsequently updated by the ground control center (Liu et al. 2014).

As a first full triple-frequency navigation system, BDS transmits B1, B2 and B3 signals, and the broadcast satellite clock bias is based on B3 signals. To keep signal coherence, a single "equipment group delay differential" TGD1 was originally defined in the B1I Open service ICD (CSNO 2012) to support the single-frequency B1 users. By the end of 2013, another "equipment group delay differential" parameter TGD2 was introduced in the second release of the ICD (CSNO 2013). Therefore, two group delay differential parameters TGD1 and TGD2 are presently provided in the BDS navigation message that describes corrections for use with B1 and B2 signals, respectively.

As an integral part of ionospheric model, GPS/GLONASS DCBs are routinely estimated by IGS Analysis Centers and reported as part of Global Ionosphere Maps (GIM) or released as independent DCB products (Feltens and Schaer 1998; Schaer 2003; Hernández-Pajares et al. 2009). As a developing constellation, BDS does not yet provide official DCB products at present. Within the Multi-GNSS Experiment (MGEX) launched by the International GNSS Service (IGS) (Dow et al. 2009), over 50 stations are now equipped with new generation multi-system receivers that can record BDS signals worldwide (Rizos et al. 2013; Dach et al. 2014). These offer a basis for the determination of BDS DCBs. Currently both BDS satellite and receiver biases from weekly averages of daily DCBs are provided in the annual files MGEX*yyyy*.bsx and MGEX*yyyy*_all.bsx, where *yyyy* indicates the four-digit year. Figure 1 shows parts of the format of DCBs extracted from the annual file "MGEX2014.bsx" (available at: ftp://cddis.gsfc.nasa.gov/pub/gps/products/mgex/dcb/).

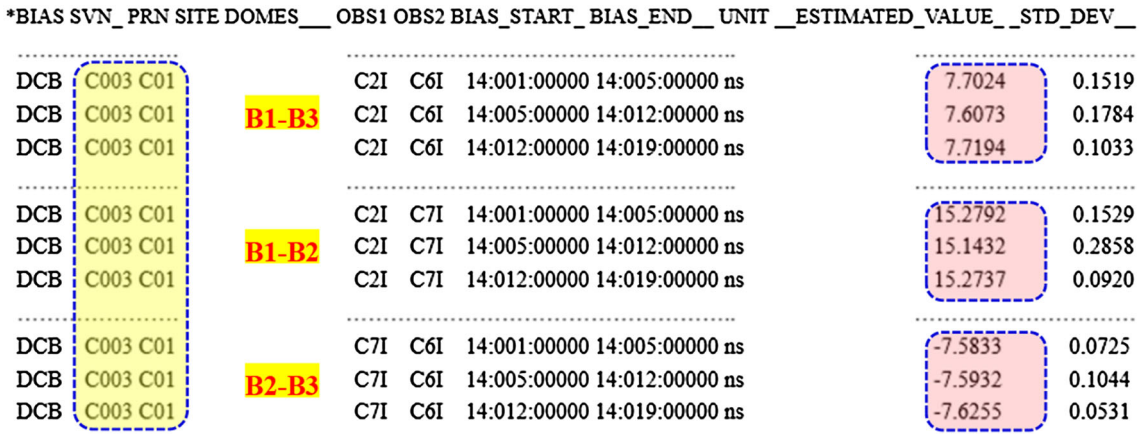


**Fig. 1** The basic format of multi-GNSS DCB products provided by MGEX

It should be noted that, C2I, C7I and C6I, respectively, represent the pseudorange observation of B1, B2 and B3 signal according to the Receiver Independent Exchange Format (RINEX 3.01, available at: http://igscb.jpl.nasa.gov/igscb/data/format/rinex301.pdf). As shown in Fig. 1, three differential code biases (C2I–C6I, C2I–C7I and C7I–C6I) of C01 satellite during the period of day of year (DOY) 001–019, 2014 are selected to show the structure of the DCB files. The estimated values of DCBs have been averaged over a few days (or weekly) time interval, and the variations are relatively small in a few weeks. The last column shows the standard deviations which reflect the scatter of daily DCBs over the averaging interval. However, it is worth mentioning that this product may be redundant but conflicting as there are only two independent DCBs among three code observables theoretically (Montenbruck et al. 2014). In other words, consistency of these biases cannot be ensured since individual biases are separately estimated with different datasets. So it is no surprising to find that DCB (B1–B3) may differ from the sum of DCB (B1–B2) and DCB (B2–B3) in Fig. 1.

Furthermore, for a span of three months (about 13 weeks from 1 January 2014), DCBs including the estimated values and standard deviations of the 14 on-orbit BDS satellites are plotted in Figs. 2, 3 and 4, and the misclosure ($\mathrm{DCB_{B1B2}} + \mathrm{DCB_{B2B3}} - \mathrm{DCB_{B1B3}}$) of each satellite is statistically calculated and shown in Fig. 5. As shown in these plots, most of the derived DCBs range from −8 to 8 ns with a variation of 0.1–0.2 ns, while a few GEO satellites like C01 and C02 show significant larger values, i.e., the value of $\mathrm{DCB_{B1B2}}$ for C01 is over 15 ns. Nevertheless, the DCB parameters run smoothly for a time span of 3 months, which means the DCBs of BDS satellites may be stable enough for a long-time prediction. Since the three DCBs ($\mathrm{DCB_{B1B2}}$, $\mathrm{DCB_{B2B3}}$ and$\mathrm{DCB_{B1B3}}$) are separately estimated with different observations, inevitable misclosure can be observed for a specific satellite. The given statistic results indicate that the self-consistency (misclosure) is better than 0.2 ns for most of satellites, with exceptions of C04 and C05. This may be attributed to their location and limited tracking range.

## 3 BDS TGD/DCB correction model

The existing TGD/DCB correction models, as well as the relationship between TGD and DCB for GPS are first reorganized here for the convenience of readers. Then the correction models for BDS are derived and extended for various occasions: correction models for either broadcast satellite clock or precise satellite clock users; correction models with either TGD or DCB parameters; correction models for any single (B1, B2, and B3) and dual-frequency (B1B2, B1B3, and B2B3) signals. Also, the relationship between TGDs and DCBs for BDS are explicitly figured out and compared against GPS in this section.

### 3.1 Pseudorange observation equations

For a specific satellite-receiver link, simplified equations of the triple-frequency range observations $P_i$ $(i = 1, 2, 3)$ can be described as (Abdel-salam 2005):

$$P_1 = \rho + \mathrm{d}\rho + I_1 + \mathrm{d}t_\mathrm{r} - \mathrm{d}t^\mathrm{s} + D_{P1} \quad (1)$$

$$P_2 = \rho + \mathrm{d}\rho + \gamma I_1 + \mathrm{d}t_\mathrm{r} - \mathrm{d}t^\mathrm{s} + D_{P2} \quad (2)$$

$$P_3 = \rho + \mathrm{d}\rho + \beta I_1 + \mathrm{d}t_\mathrm{r} - \mathrm{d}t^\mathrm{s} + D_{P3} \quad (3)$$

where $\rho$ is the true geometric range between receiver and satellite (m), $\mathrm{d}\rho$ is the range error due to satellite orbit error and tropospheric delay (m), $I_1$ is the ionospheric delay in the measured pseudorange on the first frequency (m), $\gamma$ and $\beta$ are the frequency-dependent multiplier factors ($\gamma = f_1^2/f_2^2$, $\beta = f_1^2/f_3^2$), $\mathrm{d}t_\mathrm{r}$ is the receiver clock error in the measured pseudorange (m), $\mathrm{d}t^\mathrm{s}$ is the satellite clock error in the measured pseudorange (m), $D_{P(i)}$ $(i = 1, 2, 3)$ is the instrumental (hardware) delay in the measured pseudorange (m),

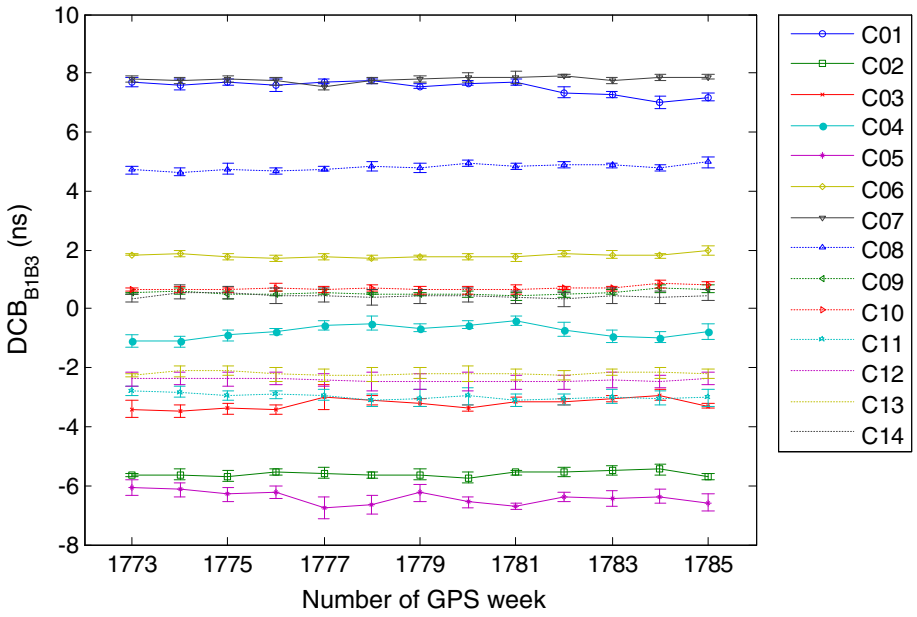


**Fig. 2** Time series of weekly $DCB_{B1B3}$

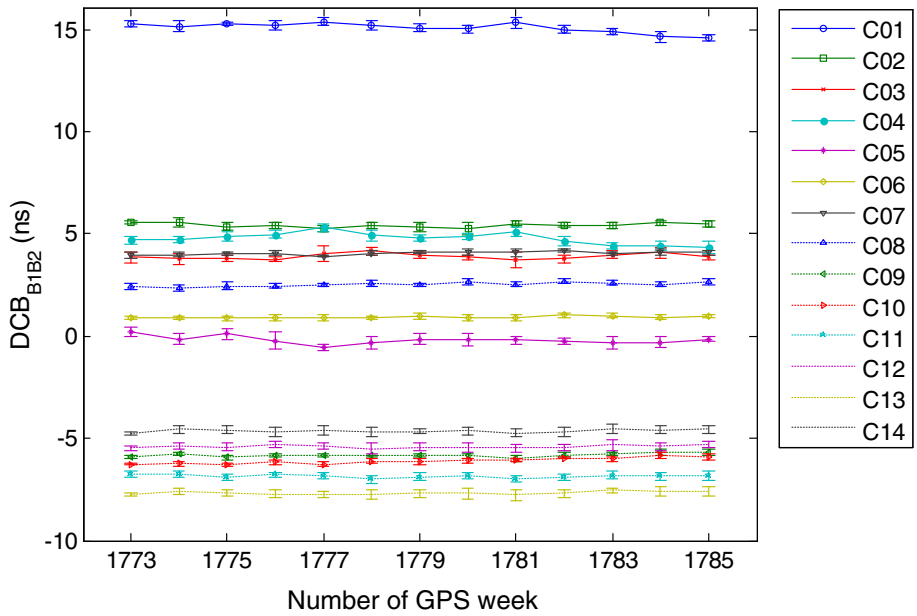


**Fig. 3** Time series of weekly $DCB_{B1B2}$

including instrumental biases on both satellite and receiver ends.

In case that the hardware delay corrections for all of the common-view satellites have a common bias, the bias will be absorbed by the receiver clock error rather than the positioning vector in the positioning applications. Therefore, the bias of receiver hardware delay is ignored, and $D_{P(i)}$ stands only for the satellite part of the delay in the following sections.

### 3.2 TGDs/DCBs correction model for GPS

By convention, the ionosphere-free linear combination (LC) of $P1$ and $P2$ pseudorange is used for satellite clock estimation, and the hardware delays are ignored during the estimation process. As such, the GPS satellite clock error $\bar{d}t^s$ provided either in the broadcast navigation message or the precise satellite clock product, contains a specific linear combination of $P1$ and $P2$ satellite biases, specifically the ionosphere-free LC (Gao 2008; Schaer 2008). That is

$$\bar{\mathrm{d}}t^{\mathrm{s}} = \mathrm{d}t^{\mathrm{s}} - \left(\frac{\gamma}{\gamma-1}D_{P1} - \frac{1}{\gamma-1}D_{P2}\right) \tag{4}$$

where $\gamma = f_1^2/f_2^2$, $f_1$ and $f_2$ are the frequency of L1 and L2 signal, respectively.

Therefore, an additional term to account for hardware delay should be applied at the single-frequency user end

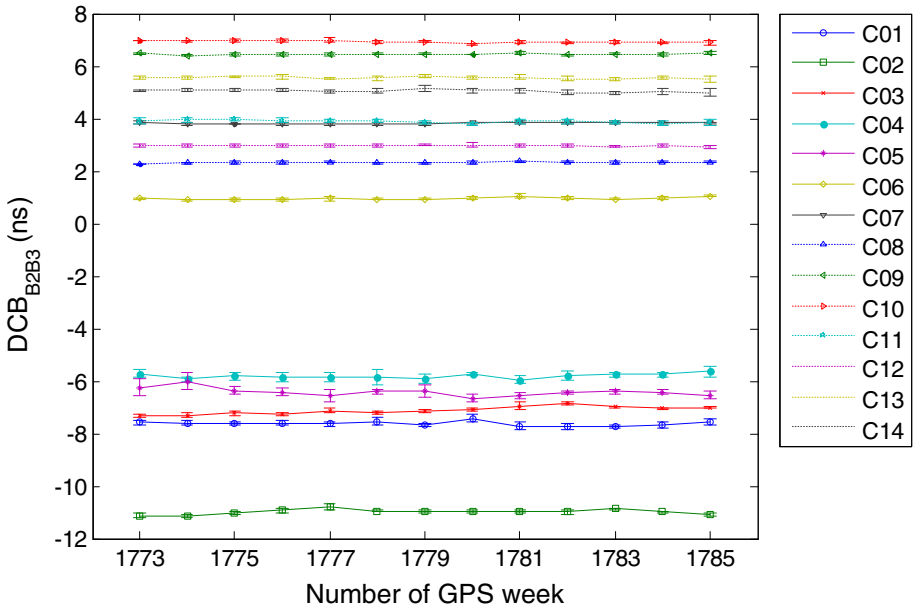


**Fig. 4** Time series of weekly $DCB_{B2B3}$

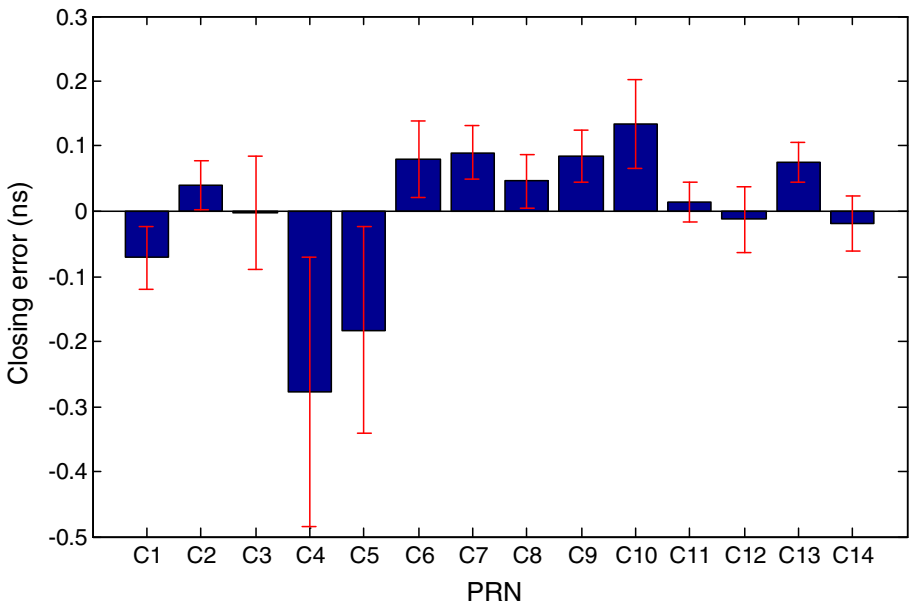


**Fig. 5** Statistic misclosure of the three DCBs ($DCB_{B1B2}$, $DCB_{B2B3}$ and $DCB_{B1B3}$ )

when using GPS satellite clock corrections. Otherwise, the clock inconsistency will propagate into the positioning solution. Substituting Eq. 4 in Eqs. 1 and 2, we get the new equations expressed as:

$$P_1 = \rho + \mathrm{d}\rho + I_1 + \mathrm{d}t_\mathrm{r} - \bar{\mathrm{d}}t^\mathrm{s} - \frac{1}{\gamma - 1}(D_{P1} - D_{P2}) \quad (5)$$

$$P_2 = \rho + \mathrm{d}\rho + \gamma I_1 + \mathrm{d}t_\mathrm{r} - \bar{\mathrm{d}}t^\mathrm{s} - \frac{\gamma}{\gamma - 1}(D_{P1} - D_{P2}) \quad (6)$$

Also, the dual-frequency ionosphere-free pseudorange combination (PC) can be written as:

$$\mathrm{PC}_{12} = \frac{\gamma \cdot P_1 - P_2}{\gamma - 1} = \rho + \mathrm{d}\rho + \mathrm{d}t_\mathrm{r} - \bar{\mathrm{d}}t^\mathrm{s} \quad (7)$$

As illustrated in Eqs. 5–7, single-frequency GPS users are required to perform instrumental bias correction while dual-frequency PC users are free of instrumental biases once the satellite clock error $\bar{\mathrm{d}}t^\mathrm{s}$ is used. However, the instrumental biases $(D_{P1}, D_{P2})$ cannot be determined in an absolute sense, so the differential code biases are used instead (Schaer 2008, 2012). It is common to denote a specific difference of code bias $\mathrm{DCB}_{(P1P2)}$ as:

$$\mathrm{DCB}_{(P1P2)} = D_{P2} - D_{P1} \quad (8)$$

In addition, the single-frequency $P1$ or $P2$ users can be corrected by the following equations with TGD parameters according to the released public GPS ICD:

$$P_1 = \rho + \mathrm{d}\rho + I_1 + \mathrm{d}t_\mathrm{r} - \bar{\mathrm{d}}t^\mathrm{s} - \mathrm{TGD} \quad (9)$$

$$P_2 = \rho + \mathrm{d}\rho + \gamma I_1 + \mathrm{d}t_\mathrm{r} - \bar{\mathrm{d}}t^\mathrm{s} - \gamma \cdot \mathrm{TGD} \quad (10)$$

Comparing Eqs. 5 and 6 with Eqs. 9 and 10 the relationship between TGD and DCB is clear as:

$$\mathrm{TGD} = \frac{1}{1-\gamma}\mathrm{DCB}_{(P1P2)} \quad (11)$$

For GPS, the value of TGD is not equal to the mean SV group delay differential, but a measured value that represents the mean group delay differential multiplied by $1/(1-\gamma)$. It is worth mentioning that, not all modern receivers can produce C/A, $P1$ and $P2$. Current Trimble and Leica receivers output $C1$ and $P2$ instead of $P1$ and $P2$ (Schaer 2012). For maximum accuracy, coarse acquisition (C/A) code observations should first be converted to keep consistency with $P1$/ $P2$ non-cross correlation types. A RINEX converter utility, cc2noncc, is provided by IGS to easily make measurements consistent with P1/P2 data by applying satellite-dependent $P1$–$C1$ bias corrections (Ray 2001). Detailed correction terms for various observations refer to Schaer (2008, 2012).

### 3.3 TGD/DCB correction model for BDS

Despite a similarity of names and similar application in navigation, users should be aware that the BDS group delay parameters are conceptually different from the common "timing group delay" parameters employed in GPS. This difference is vital for a proper processing of any single-frequency observation and linear combinations of code observations on multiple frequencies.

#### *3.3.1 Correction model with broadcast satellite clocks*

Unlike GPS, BDS broadcast satellite clock corrections are referred to the B3 signal rather than dual-frequency ionosphere-free LC. Satellite clock errors provided in the navigation message ($\bar{\mathrm{d}}t^\mathrm{s}_\mathrm{brd}$) contain a specific P3 satellite bias. That is

$$\bar{\mathrm{d}}t^\mathrm{s}_\mathrm{brd} = \mathrm{d}t^\mathrm{s} - D_{P3} \quad (12)$$

By substitution of Eq. 12 into Eqs. 1–3 and taking into account the definition of DCBs, the single-frequency pseudorange of BDS can be written as (Montenbruck and Steigenberger 2013):

$$P_1 = \rho + \mathrm{d}\rho + I_1 + \mathrm{d}t_\mathrm{r} - \bar{\mathrm{d}}t^\mathrm{s}_\mathrm{brd} - \mathrm{DCB}_{(P1P3)} \quad (13)$$

$$P_2 = \rho + \mathrm{d}\rho + \gamma I_1 + \mathrm{d}t_\mathrm{r} - \bar{\mathrm{d}}t^\mathrm{s}_\mathrm{brd} - \mathrm{DCB}_{(P2P3)} \quad (14)$$

$$P_3 = \rho + \mathrm{d}\rho + \beta I_1 + \mathrm{d}t_\mathrm{r} - \bar{\mathrm{d}}t^\mathrm{s}_\mathrm{brd} \quad (15)$$

where $\gamma = f_1^2/f_2^2$, $\beta = f_1^2/f_3^2$, $f_1$, $f_2$ and $f_3$ are the frequencies of B1, B2 and B3 signal, respectively. Furthermore, pseudoranges on B1 and B2 can be corrected by the following equations according to latest released BDS ICD:

$$P_1 = \rho + \mathrm{d}\rho + I_1 + \mathrm{d}t_\mathrm{r} - \bar{\mathrm{d}}t^\mathrm{s}_\mathrm{brd} - \mathrm{TGD}_1 \quad (16)$$

$$P_2 = \rho + \mathrm{d}\rho + \gamma I_1 + \mathrm{d}t_\mathrm{r} - \bar{\mathrm{d}}t^\mathrm{s}_\mathrm{brd} - \mathrm{TGD}_2 \quad (17)$$

Similarly, the following relationship between the TGDs and DCBs can be obtained by comparing Eqs. 13 and 14 with Eqs. 16 and 17:

$$\mathrm{TGD}_1 = \mathrm{DCB}_{(P1P3)} \quad (18)$$

$$\mathrm{TGD}_2 = \mathrm{DCB}_{(P2P3)} \quad (19)$$

Therefore, the meaning of BDS TGDs is different from that of GPS TGD, and the value of BDS TGD should be equal to the mean SV group delay differential rather than the value multiplied by a frequency-dependent factor. But, we should be aware that the DCBs cannot be directly compared with TGDs since zero-mean (or fixed) constraint equations are imposed to solve the rank deficiency during the DCB estimations. For comparison, all TGDs are normalized to a zero constellation average, and Fig. 6 shows the comparison of broadcast $\mathrm{TGD}_1$ and $\mathrm{TGD}_2$ group delay parameters with B1–B3 and B2–B3 differential code biases ($\mathrm{DCB}_{13}$ and $\mathrm{DCB}_{23}$) provided by MGEX on 16 February 2014. The differences between TGDs and DCBs are also plotted with red bars for each satellite, and the root mean squares are calculated based on the whole constellation (14 satellites).

As shown in Fig. 6, the broadcast TGD parameters agree well with the DCB parameters from MEGX. The RMS of the differences are better than 2 nanoseconds, which clearly support the relationship between TGDs and DCBs for BDS. Thus $\mathrm{TGD}_1$ and $\mathrm{TGD}_2$ can be, respectively, interpreted as B1–B3 and B2–B3 differential code biases. But it is interesting to find that the consistency between $\mathrm{TGD}_2$ and $\mathrm{DCB}_{23}$ parameters is much better than the consistency between $\mathrm{TGD}_1$ and $\mathrm{DCB}_{13}$ parameters. This might be attributed to the smaller frequency difference of about 60 MHz for B2/B3 compared to about 300 MHz for B1/B3. Further analyses are required to better understand these phenomena.

For dual-frequency users, three ionosphere-free LCs take the following derivations:

$$\mathrm{PC}_{12} = \rho + \mathrm{d}\rho + \mathrm{d}t_\mathrm{r} - \bar{\mathrm{d}}t^\mathrm{s}_\mathrm{brd} - \left[\frac{\gamma}{\gamma-1}\mathrm{DCB}_{(P1P3)} - \frac{1}{\gamma-1}\mathrm{DCB}_{(P2P3)}\right] \quad (20)$$

$$\mathrm{PC}_{13} = \rho + \mathrm{d}\rho + \mathrm{d}t_\mathrm{r} - \bar{\mathrm{d}}t^\mathrm{s}_\mathrm{brd} - \frac{\beta}{\beta-1}\mathrm{DCB}_{(P1P3)} \quad (21)$$

$$\mathrm{PC}_{23} = \rho + \mathrm{d}\rho + \mathrm{d}t_\mathrm{r} - \bar{\mathrm{d}}t^\mathrm{s}_\mathrm{brd} - \frac{\kappa}{\kappa-1}\mathrm{DCB}_{(P2P3)} \quad (22)$$

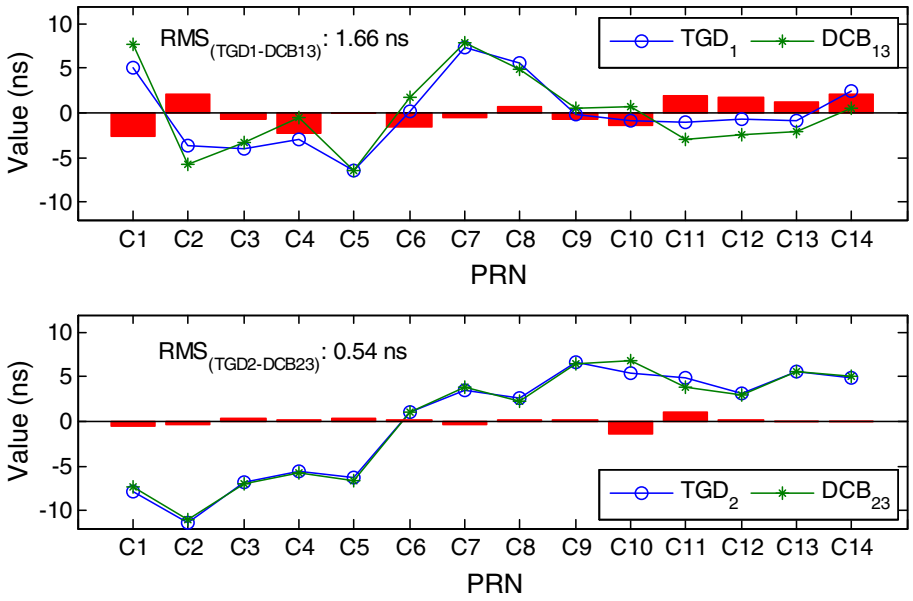


**Fig. 6** Comparison of broadcast TGDs with MGEX DCBs (TGDs are normalized to zero mean)

where $\kappa = f_2^2/f_3^2$, and the DCB parameters can be replaced by TGDs according to Eqs. 18 and 19. As shown in the above Eqs. (13–22), TGDs/DCBs need to be applied both in B1 and B2 single-frequency application as well as B1/B2, B1/B3 or B2/B3 dual-frequency application.

### *3.3.2 Correction model with precise satellite clocks*

Currently, the precise satellite orbit and clock products of BDS provided by MGEX are derived from the B1/B2 ionosphere-free LC, and consequently the precise satellite clock error $\bar{\mathrm{d}}t^{\mathrm{s}}_{\mathrm{pre}}$ plays the same role as $\bar{\mathrm{d}}t^{\mathrm{s}}$ in Eq. 4. Accordingly, the corrected pseudoranges for B1, B2 and B3 single-frequency users can be described as:

$$P_1 = \rho + \mathrm{d}\rho + I_1 + \mathrm{d}t_{\mathrm{r}} - \bar{\mathrm{d}}t^{\mathrm{s}}_{\mathrm{pre}} + \frac{1}{\gamma - 1}\mathrm{DCB}_{(P1P2)} \quad (23)$$

$$P_2 = \rho + \mathrm{d}\rho + \gamma I_1 + \mathrm{d}t_{\mathrm{r}} - \bar{\mathrm{d}}t^{\mathrm{s}}_{\mathrm{pre}} + \frac{\gamma}{\gamma - 1}\mathrm{DCB}_{(P1P2)} \quad (24)$$

$$P_3 = \rho + \mathrm{d}\rho + I_1 + \mathrm{d}t_{\mathrm{r}} - \bar{\mathrm{d}}t^{\mathrm{s}}_{\mathrm{pre}} + \left[\frac{\gamma}{\gamma - 1}\mathrm{DCB}_{(P1P3)} - \frac{1}{\gamma - 1}\mathrm{DCB}_{(P2P3)}\right] \quad (25)$$

For dual-frequency users, the DCB corrections are derived as:

$$\mathrm{PC}_{12} = \rho + \mathrm{d}\rho + \mathrm{d}t_{\mathrm{r}} - \bar{\mathrm{d}}t^{\mathrm{s}}_{\mathrm{pre}} \quad (26)$$

$$\mathrm{PC}_{13} = \rho + \mathrm{d}\rho + \mathrm{d}t_{\mathrm{r}} - \bar{\mathrm{d}}t^{\mathrm{s}}_{\mathrm{pre}} - \left[\frac{1}{\beta - 1}\mathrm{DCB}_{(P1P3)} - \frac{1}{\gamma - 1}\mathrm{DCB}_{(P1P2)}\right] \quad (27)$$

$$\mathrm{PC}_{23} = \rho + \mathrm{d}\rho + \mathrm{d}t_{\mathrm{r}} - \bar{\mathrm{d}}t^{\mathrm{s}}_{\mathrm{pre}} - \left[\frac{1}{\kappa - 1}\mathrm{DCB}_{(P2P3)} - \frac{\gamma}{\gamma - 1}\mathrm{DCB}_{(P1P2)}\right] \quad (28)$$

Also, the above corrections can use TGDs instead of DCBs if no DCB products are available. The DCB parameters $\mathrm{DCB}_{(P1P3)}$ and $\mathrm{DCB}_{(P2P3)}$ can be substituted directly by TGD1 and TGD2, respectively, and $\mathrm{DCB}_{(P1P2)}$ can be expressed as a linear combination of the other two parameters:

$$\mathrm{DCB}_{(P1P2)} = \mathrm{DCB}_{(P1P3)} - \mathrm{DCB}_{(P2P3)} = \mathrm{TGD}_1 - \mathrm{TGD}_2 \quad (29)$$

However, one should be aware that direct use of a DCB/TGD for a given signal pair is expected to better represent the pseudorange observations than chaining of multiple DCBs/TGDs.

## 3.4 Summary of TGD/DCB correction models for BDS

For simplicity, let

$$\bar{\rho} = \rho + \mathrm{d}\rho + \mathrm{d}t_{\mathrm{r}} - \bar{\mathrm{d}}t^{\mathrm{s}} \quad (30)$$

The TGD/DCB correction models for single- and dual-frequency users with broadcast satellite clock $\bar{\mathrm{d}}t^{\mathrm{s}}_{\mathrm{brd}}$ or precise satellite clock $\bar{\mathrm{d}}t^{\mathrm{s}}_{\mathrm{pre}}$ are summarized in the following two sets of equations, which cover almost all the occasions of BDS positioning.

$$\bar{\mathrm{d}}t^{s}_{\mathrm{brd}}\begin{cases} P_1 = \bar{\rho} + I_1 - \mathrm{TGD}_1 \equiv \bar{\rho} + I_1 - \mathrm{DCB}_{(P1P3)} \\ P_2 = \bar{\rho} + \gamma I_1 - \mathrm{TGD}_2 \equiv \bar{\rho} + \gamma I_1 - \mathrm{DCB}_{(P2P3)} \\ P_3 = \bar{\rho} + \beta I_1 \\ \mathrm{PC}_{12} = \bar{\rho} - \left[\frac{\gamma}{\gamma-1}\mathrm{TGD}_1 - \frac{1}{\gamma-1}\mathrm{TGD}_2\right] \\ \qquad \equiv \bar{\rho} - \left[\frac{\gamma}{\gamma-1}\mathrm{DCB}_{(P1P3)} - \frac{1}{\gamma-1}\mathrm{DCB}_{(P2P3)}\right] \\ \mathrm{PC}_{13} = \bar{\rho} - \frac{\beta}{\beta-1}\mathrm{TGD}_1 \equiv \bar{\rho} - \frac{\beta}{\beta-1}\mathrm{DCB}_{(P1P3)} \\ \mathrm{PC}_{23} = \bar{\rho} - \frac{\kappa}{\kappa-1}\mathrm{TGD}_2 \equiv \bar{\rho} - \frac{\kappa}{\kappa-1}\mathrm{DCB}_{(P2P3)} \end{cases} \tag{31}$$

$$\bar{\mathrm{d}}t^{s}_{\mathrm{pre}}\begin{cases} P_1 = \bar{\rho} + I_1 + \frac{1}{\gamma-1}\mathrm{DCB}_{(P1P2)} \\ \qquad \equiv \bar{\rho}_{+} I_1 + \frac{1}{\gamma-1}(\mathrm{TGD}_1 - \mathrm{TGD}_2) \\ P_2 = \bar{\rho} + \gamma I_1 + \frac{\gamma}{\gamma-1}\mathrm{DCB}_{(P1P2)} \\ \qquad \equiv \bar{\rho}_{+} \gamma I_1 + \frac{\gamma}{\gamma-1}(\mathrm{TGD}_1 - \mathrm{TGD}_2) \\ P_3 = \bar{\rho}_{+} \beta I_1 + \left[\frac{\gamma}{\gamma-1}\mathrm{DCB}_{(P1P3)} - \frac{1}{\gamma-1}\mathrm{DCB}_{(P2P3)}\right] \\ \qquad \equiv \bar{\rho}_{+} \beta I_1 + \left[\frac{\gamma}{\gamma-1}\mathrm{TGD}_1 - \frac{1}{\gamma-1}\mathrm{TGD}_2\right] \\ \mathrm{PC}_{12} = \bar{\rho} \\ \mathrm{PC}_{13} = \bar{\rho} - \left[\frac{1}{\beta-1}\mathrm{DCB}_{(P1P3)} - \frac{1}{\gamma-1}\mathrm{DCB}_{(P1P2)}\right] \\ \qquad \equiv \bar{\rho} - \left[\left(\frac{1}{\beta-1} - \frac{1}{\gamma-1}\right)\mathrm{TGD}_1 + \frac{1}{\gamma-1}\mathrm{TGD}_2\right] \\ \mathrm{PC}_{23} = \bar{\rho} - \left[\frac{1}{\kappa-1}\mathrm{DCB}_{(P2P3)} - \frac{\gamma}{\gamma-1}\mathrm{DCB}_{(P1P2)}\right] \\ \qquad \equiv \bar{\rho} - \left[\frac{\gamma}{1-\gamma}\mathrm{TGD}_1 + \left(\frac{1}{\kappa-1} + \frac{\gamma}{\gamma-1}\right)\mathrm{TGD}_2\right] \end{cases} \tag{32}$$

As illustrated in Eqs. 31 and 32, for use with other signals or signal combinations which are not used as the BDS satellite clock reference, care must be taken to handle with the biases of pseudoranges introduced by the satellite clock error. The pseudoranges could be corrected with either TGD or DCB parameters depending on the occasion. For real-time applications, i.e., standard point positioning (SPP), it is common to use the broadcast satellite clock corrections and TGDs from the navigation message. For those high-accuracy pursuing users, i.e., precise point positioning (PPP), which utilizes precise satellite ephemeris and clock corrections, the DCBs are commonly applied to balance the biases of pseudorange observations. As we have mentioned above, the DCBs are systematically biased from the TGDs with constant offsets, and thus the value of $\mathrm{TGD}_1$ and $\mathrm{TGD}_2$ will not be equal to the value of $\mathrm{DCB}_{13}$ and $\mathrm{DCB}_{23}$, respectively. Fortunately, it does not matter to the positioning applications since the common code biases of the whole constellation will absolutely be absorbed by receiver clock offsets.

## 4 Validations

### 4.1 Data and processing strategy

To test the effectiveness of the TGDs/DCBs correction models as summarized in Sect. 3, four Asia-pacific regional distributed MGEX stations, namely CUT0, GMSD, JFNG and NNOR, were used for verification. A few weeks BDS dataset (1–28 February 2014) at an interval of 30 s was retrieved from each station. Table 1 lists some basic information of the tracking stations used in this paper, including the approximate location, receiver type and recorded signals. Figure 7 shows a daily variation of visible BDS satellite number (SN) and positioning dilution of precision (PDOP) value on 16 February 2014.

The dataset was processed in the mode of SPP and PPP using the updated TriP software developed by Wuhan University (Zhang et al. 2006). The precision of BDS pseudorange and carrier phase observations were assumed to be 3 m and 3 mm, respectively. The elevation cutoff angle was set to 10°, and the positioning results were compared with the daily station solutions from GFZ. Since the coordinates of NNOR were not provided by GFZ, daily solutions of GPS static PPP were used as reference coordinates. In general, the reference coordinates have an accuracy of few millimeters. For SPP, only the pseudorange observations and broadcast navigation messages were used at the user end. The ionospheric delays were corrected by Klobuchar model. Four parameters including three coordinates and one receiver clock bias were estimated as white noise process. For PPP, ionosphere-free pseudoranges as well as carrier phases were simultaneously processed (Kouba and Hérous 2001). The precise orbit and clock products at intervals of 15 and 5 min, respectively, provided by GFZ were used to remove the orbit and clock errors (Deng et al. 2014). Tropospheric delays of the dry component were corrected by Saastamoinen model, while the zenith wet

**Table 1** Basic information of the tracking stations

| Site ID | Country | Longitude | Latitude | Receiver | BDS signal |
|---|---|---|---|---|---|
| CUT0 | Australia | 115.89 | −32.00 | TRIMBLE NETR9 | B1/B2/B3 |
| GMSD | Japan | 131.02 | 30.56 | TRIMBLE NETR9 | B1/B2/B3 |
| JFNG | China | 114.49 | 30.52 | TRIMBLE NETR9 | B1/B2/B3 |
| NNOR | Australia | 116.19 | −31.05 | SEPT POLARX4 | B1/B2 |

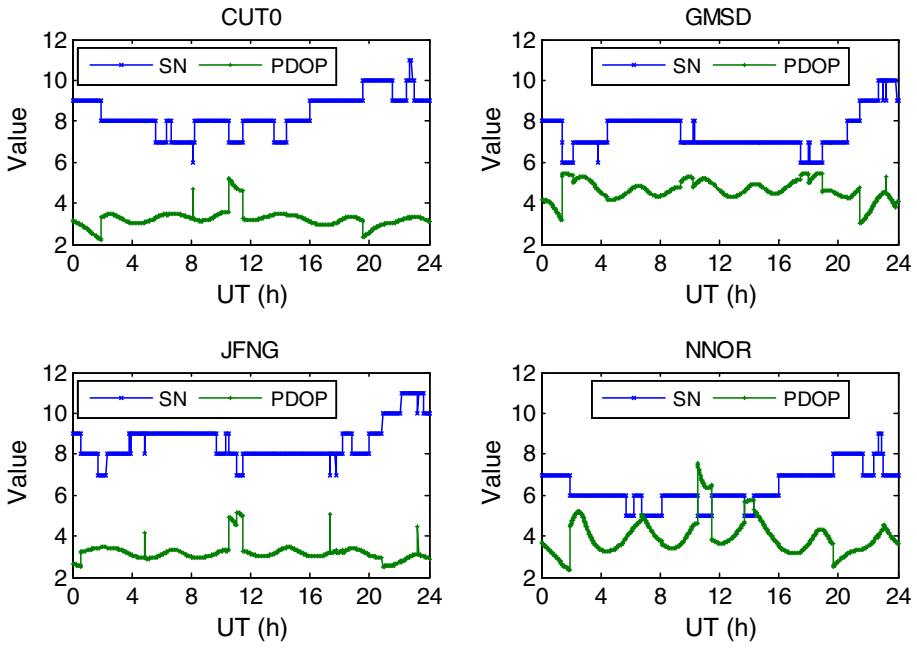


**Fig. 7** Time series of visible BDS satellites number (SN) and PDOP (16 February 2014)

**Table 2** Summary of the processing strategy

| Proc. mode | Combinations | Schemes | Comments |
|---|---|---|---|
| SPP | Single-freq: B1, B2, B3; dual-freq: B1B2, B1B3, B2B3 | 1: *non-corr*<br>2: *tgd-corr*<br>3: *dcb-corr* | *non-corr*: pseudorange without TGDs or DCBs correction; *tgd-corr*: pseudorange code bias correction with TGD parameters in navigation message; *dcb-corr*: pseudorange code bias correction with DCB parameters from MGEX |
| PPP | Dual-freq: B1B2, B1B3, B2B3 | 1: *non-corr*<br>2: *tgd-corr*<br>3: *dcb-corr* | |

tropospheric delays were estimated as random walk process. Antenna phase center offset (PCO) and phase center variation (PCV) were corrected by the absolute antenna model. But, it is worth mentioning that, only the conventional satellite PCO (+0.6, +0.0, +1.1 m) values as recommended by MGEX were applied for BDS satellite PCO correction leaving the receiver antenna PCO and PCV uncorrected (Rizos et al. 2013; Li et al. 2014). Carrier phase wind-up corrections were given in Wu et al. (1993). Remaining errors (effects), such as relativity, solid earth tides, and ocean tides, were accounted for as recommended by IERS Conventions 2010 (Petit and Luzum 2010). For each epoch, three coordinates together with epoch-wise receiver clock bias, wet tropospheric zenith delay(s), as well as float ambiguities were estimated using a Kalman filter.

To investigate the influence of code biases on positioning, three different schemes as described in Table 2 were designed for each solution. For SPP, not only the single-frequency (B1-, B2- and B3-based) pseudoranges but also the dual-frequency (B1B2, B1B3 and B2B3 ionosphere-free) combinations were used for tests. However, only three dual-frequency (B1B2, B1B3 and B2B3 ionosphere-free) combinations were processed in PPP mode to achieve the best position accuracy.

## 4.2 Performances of standard point positioning

### *4.2.1 Single-frequency SPP*

Figures 8, 9, 10, 11 and 12 show the positioning errors of one particular day (16 February 2014) for the east, north and up component of B1-, B2- and B3-signal-based SPP for CUT0, GMSD, JFNG and NNOR stations. The root mean square (RMS) errors of the single-frequency point positioning are calculated, and the mean values of the four stations are summarized in Table 3. As shown in Figs. 8, 9, 10, 11 and 12 and Table 3, meter-level positioning accuracy can be achieved by single-frequency SPP in the Asia-pacific region based on the currently deployed BDS. For the B1- and B2-based SPP, solutions of the first scheme in which the differential code biases are ignored ("non-corr") systematically deviate from the true positions. The horizontal (east and north components) RMS errors reach 2–3 m, and the vertical (up component) RMS error is about 5 m. Significant improvements can be seen

in the other two schemes ("tgd-corr" and "dcb-corr") where the code biases are corrected with TGD or DCB parameters. The positioning accuracy reaches 1–2 m horizontally and 3–4 m vertically after the code bias correction and the positioning results of the latter two schemes are very close to each other. For the B3-based SPP, the positioning results are unaffected by the differential code biases since the broadcast satellite clock corrections refer to B3 pseudoranges. In addition, due to the lack of B3 signals on NNOR station, the B3 SPP was conducted only on the other three stations with the first scheme, and the positioning errors are shown in Fig. 12 and Table 3.

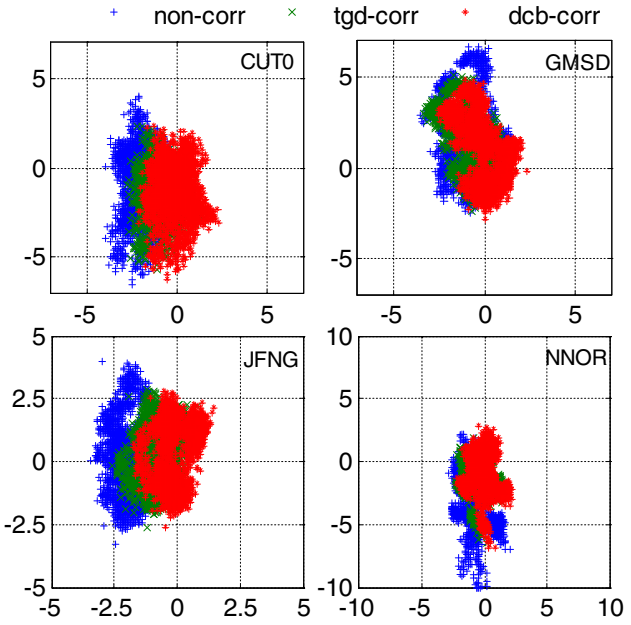


**Fig. 8** Horizontal positioning error scatters of B1 SPP with different schemes. For each plot, the *horizontal* and *vertical axis* represents, respectively, the east and north component error (unit: m)

### 4.2.2 Dual-frequency SPP

Figures 13, 14 and 15 show the histograms of the positioning error of B1B2 ionosphere-free combined SPP on JFNG station. One should be aware that the horizontal scales/ranges may be different for the three different schemes in the same figure. SPP results with B1B2, B1B3 and B2B3 combinations on other stations show the similar feature and thus not be presented herein. The statistical results (RMS error) of all dual-frequency SPP tests are given in Table 4.

As can be seen in Figs. 13, 14, 15 and Table 4, the positioning accuracy can be evidently improved by the TGD/DCB corrections. Comparing with the first scheme ("non-corr"), the other two schemes ("tgd-corr" and "dcb-corr") show more reasonable error distributions, and the third scheme ("dcb-corr") is slightly better than the second one ("tgd-corr"). Actually, this may be attributed to the more accurate DCB products provided by MGEX. Comparing Table 4 with Table 3, one can notice that the positioning accuracies of dual-frequency SPP are even worse than that of single-frequency, particularly the B2B3-based SPP. This is reasonable when we acknowledge the fact that the observation noise (TGD/DCB parameter errors included) of the dual-frequency LCs is significantly enlarged by different factors. The B1B2- and B1B3-based SPPs have the combination coefficients [2.4872, −1.4872] and [2.9437, −1.9437], and thus the noise amplification factors are 2.9 and 3.5, respectively. For the B2B3-based SPP, the ionosphere-free combination coefficient is [−9.590, 10.590], and the corresponding amplification factor reaches 14.3. Consequently, the accuracy of dual-frequency SPP is significantly degraded, particularly

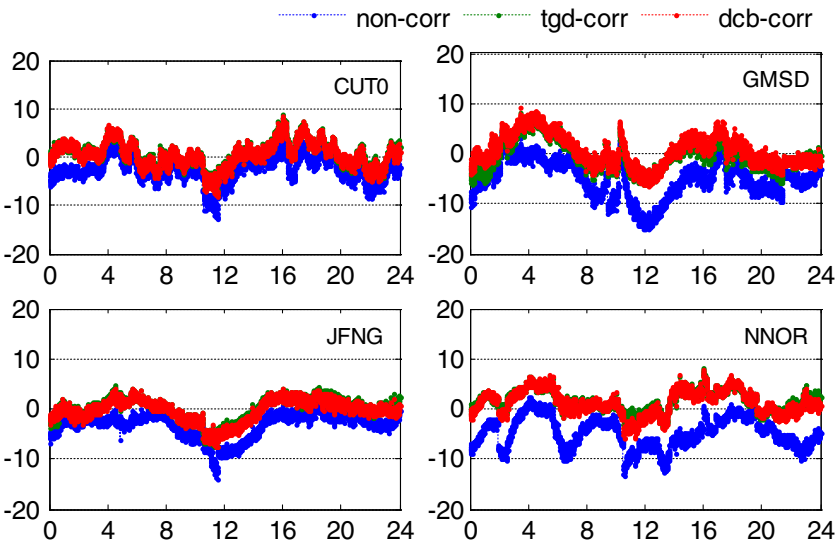


**Fig. 9** Vertical positioning error series of B1 SPP with different schemes. For each plot, the *horizontal axis* represents the universal time (unit: h), and the *vertical axis* represents the positioning error of up component (unit: m)

for the B2B3 dual-frequency combination. Nevertheless, an accuracy of 1–2 m in horizontal and 3–5 m in vertical is achieved at the user end when the B1B2- and B1B3-based SPPs are conducted.

### 4.3 Performances of precise point positioning

As mentioned in Sect. 3, the precise satellite clock corrections refer to B1B2 ionosphere-free LC, and the positioning results are unaffected by the differential code biases. Therefore, only the first scheme was performed for the B1B2-based PPP, and the kinematic (epoch-wise) PPP solutions of the four stations are shown in Fig. 16. Figures 17 and 18 show the positioning results of B1B3- and B2B3-based PPP on CUT0 and JFNG stations. Furthermore, the positioning accuracies of all the PPP tests after convergence are calculated and summarized in Table 5.

As shown in Figs. 16, 17, 18 and Table 5, the B1B2-based PPP shows the best performance, while the B2B3-based PPP shows the worst performance. The positioning accuracy reaches a few centimeters (mostly 2–3 cm) in horizontal and 7–8 cm in vertical for the B1B2-based PPP. The accuracy of B1B3-based PPP is slightly worse than that of B1B2 PPP. However, the accuracy of the B2B3-based PPP is worse by a factor of 2–3. This is reasonable when we acknowledge the fact that the noise amplification factor of the three ionosphere-free combinations is different. It should be pointed out that the current BDS-only PPP still has a great potential for further improvements. Presently, no precise PCO and PCV corrections are now available for BDS satellites and receivers. As a developing system, the quality of BDS satellite orbit and clock products is a matter of concern, particularly for those GEO satellites due to the poor distribution of ground tracking stations. Currently, only a few ACs intermittently provide BDS orbits and clocks with different quality. In other words, no final combined BDS orbit and clock products are available now. Moreover, the precise clock corrections for BDS are given in 5 min (rather than 30 s or higher) interval, which cannot satisfy the high rate kinematic applications.

For the B1B3-based PPP, the epoch-wise coordinate difference between the first scheme ("non-corr") and the third scheme ("dcb-corr") reaches a few centimeters at the first

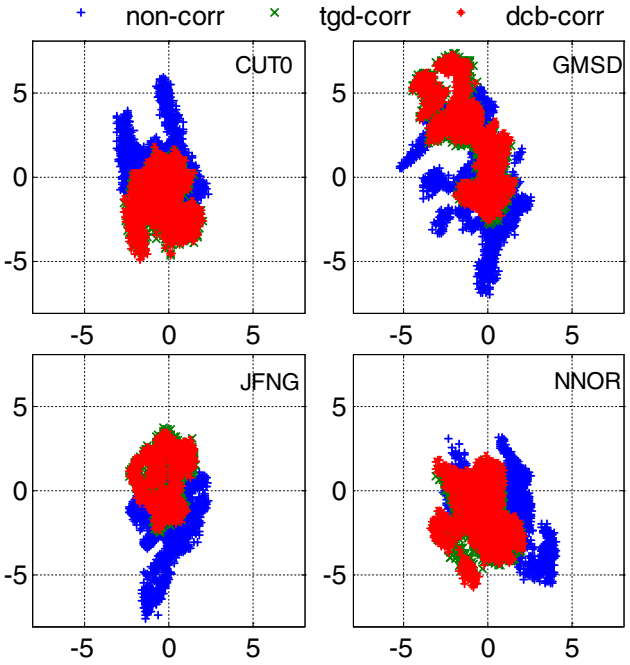


**Fig. 10** Horizontal positioning error scatters of B2 SPP with different schemes. For each plot, the *horizontal* and *vertical axes* represent, respectively, the east and north component error (unit: m)

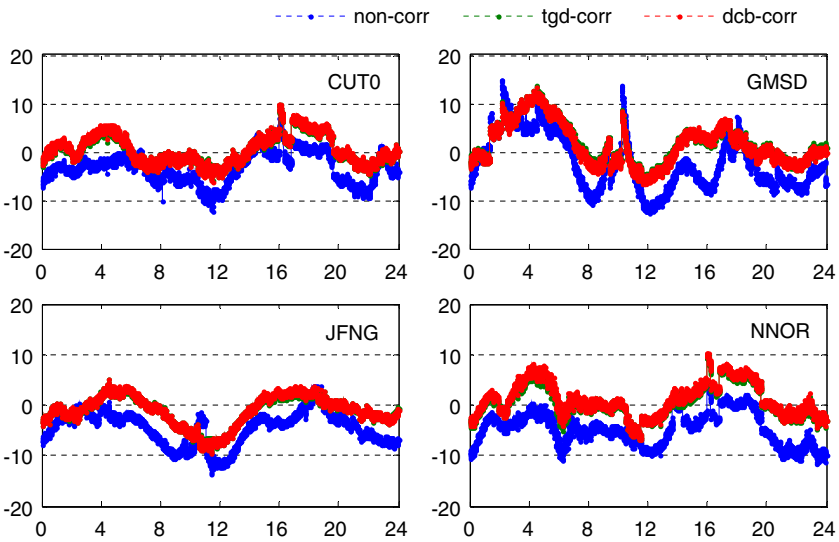


**Fig. 11** Vertical positioning error series of B2 SPP with different schemes. For each plot, the *horizontal axis* represents the universal time (unit: h), and the *vertical axis* represents the positioning error of up component (unit: m)

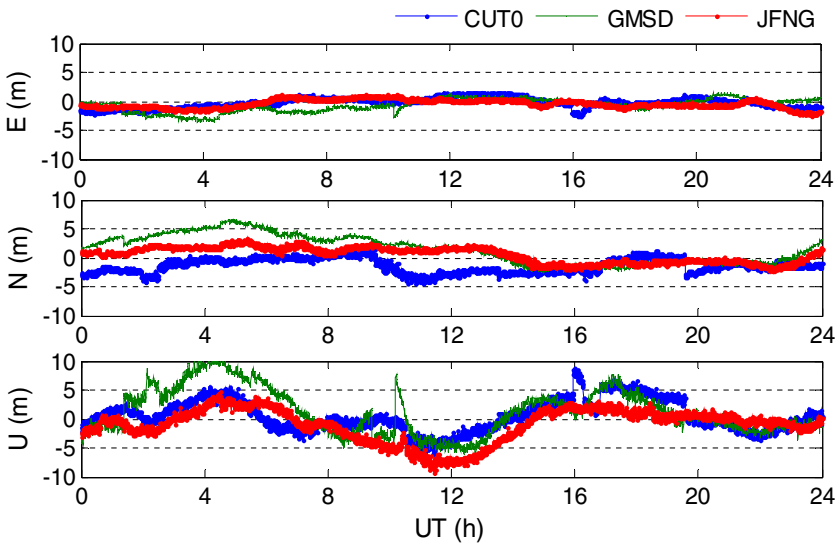


**Fig. 12** Positioning error series of B3 SPP. The *upper*, *middle* and *lower plots* show, respectively, the error of east, north and up component

**Table 3** Root mean squares of single-frequency standard point positioning (m)

| Scheme | B1-SPP | | | B2-SPP | | | B3-SPP | | |
|---|---|---|---|---|---|---|---|---|---|
| | East | North | Up | East | North | Up | East | North | Up |
| non-corr[1] | 1.638 | 2.434 | 4.873 | 1.420 | 2.172 | 5.452 | 1.011 | 2.053 | 3.289 |
| tgd-corr[2] | 1.014 | 1.605 | 2.637 | 1.143 | 2.115 | 3.481 | – | – | – |
| dcb-corr[3] | 0.776 | 1.712 | 2.682 | 1.146 | 2.137 | 3.415 | – | – | – |
| Improv$^{2-1}$ (%) | 38.1 | 34.1 | 45.9 | 19.5 | 2.6 | 36.2 | – | – | – |
| Improv$^{3-1}$ (%) | 52.6 | 29.7 | 45.0 | 19.3 | 1.6 | 37.4 | – | – | – |

$\text{Improv}^{2-1} = |\text{RMS}_{\text{non-corr}} - \text{RMS}_{\text{tgd-corr}}|/\text{RMS}_{\text{non-corr}}$; $\text{Improv}^{3-1} = |\text{RMS}_{\text{non-corr}} - \text{RMS}_{\text{dcb-corr}}|/\text{RMS}_{\text{non-corr}}$

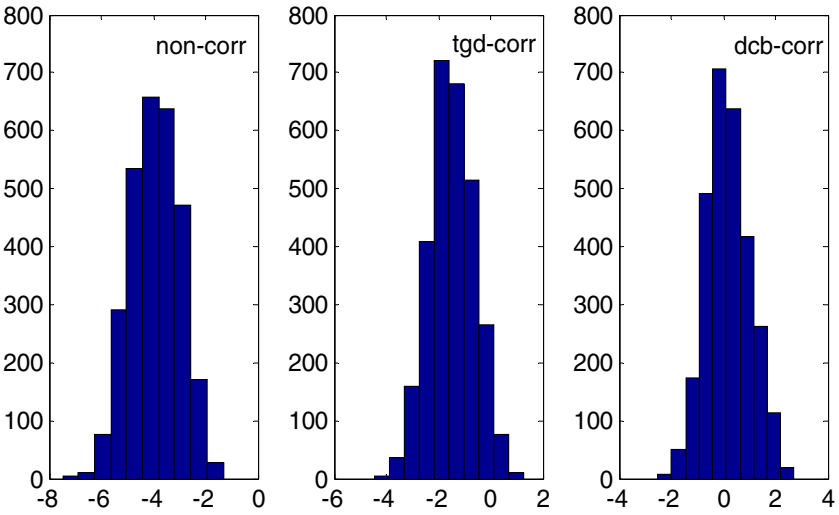


**Fig. 13** Histograms of the positioning error (east component) of B1B2 SPP on JFNG site. For each plot, the *horizontal axis* represents the positioning error (unit: m), and the *vertical axis* represents the number of samples

few hours. After a few hours smoothing, the differences are significantly decreased to a few millimeters in horizontal and 1 cm in vertical. The second scheme ("tgd-corr") shows the same feature but with much smaller differences with respect to the third scheme. In other words, the differential code biases could be effectively mitigated using either TGD or DCB parameters. For the B2B3-based PPP, the coordinate differences between the second and third schemes are mostly less than 2–3 cm, whereas the differences between the first and third schemes are over 0.2 m at the initial stage. Thanks to the increasing contribution of high-accurate carrier phases in the following epochs, finally all the three schemes

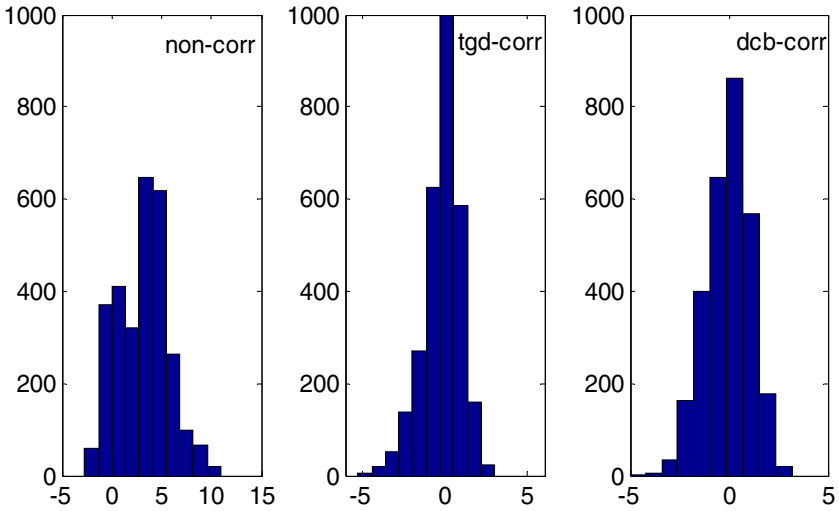


**Fig. 14** Histograms of the positioning error (north component) of B1B2 SPP on JFNG site. For each plot, the *horizontal axis* represents the positioning error (unit: m), and the *vertical axis* represents the number of samples

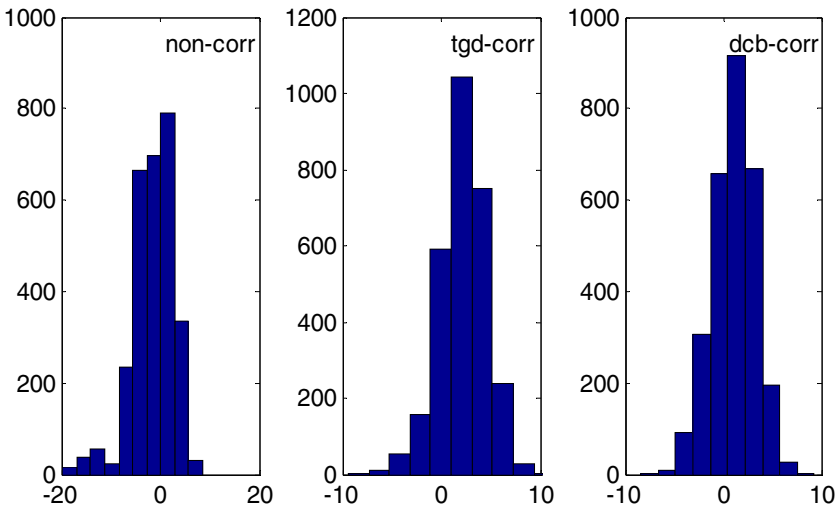


**Fig. 15** Histograms of the positioning error (up component) of B1B2 SPP on JFNG site. For each plot, the *horizontal axis* represents the positioning error (unit: m), and the *vertical axis* represents the number of samples

**Table 4** Root mean squares of dual-frequency standard point positioning (m)

| Scheme | B1B2-SPP | | | B1B3-SPP | | | B2B3-SPP | | |
|---|---|---|---|---|---|---|---|---|---|
| | East | North | Up | East | North | Up | East | North | Up |
| non-corr[1] | 3.445 | 5.741 | 6.492 | 3.662 | 3.149 | 9.378 | 6.440 | 25.765 | 42.540 |
| tgd-corr[2] | 1.503 | 1.588 | 4.196 | 1.780 | 1.824 | 4.402 | 3.242 | 4.143 | 8.950 |
| dcb-corr[3] | 1.188 | 1.631 | 3.228 | 1.422 | 1.717 | 3.509 | 3.215 | 3.451 | 8.499 |
| Improv$^{2-1}$ (%) | 56.4 | 72.3 | 35.4 | 51.4 | 42.1 | 53.1 | 49.7 | 83.9 | 79.0 |
| Improv$^{3-1}$ (%) | 65.5 | 71.6 | 50.3 | 61.2 | 45.5 | 62.6 | 50.1 | 86.6 | 80.0 |

Improv$^{2-1}$ $= |\text{RMS}_{\text{non-corr}} - \text{RMS}_{\text{tgd-corr}}|/\text{RMS}_{\text{non-corr}}$; Improv$^{3-1}$ $= |\text{RMS}_{\text{non-corr}} - \text{RMS}_{\text{dcb-corr}}|/\text{RMS}_{\text{non-corr}}$

get an accuracy of 0.1 m in horizontal and 0.2 m vertically.

Even though the impacts of differential code biases are smoothed by increasing epochs, it is unwise to ignore the differential code biases since the biases will be absorbed by other estimates or reflected in the residuals. Even worse, they may influence the PPP convergence and ambiguity resolution. Take GMSD for example, Fig. 19 shows the pseudorange residuals of B1B3 PPP, and Fig. 20 shows the B1B3 PPP solutions of the first 1 h. Sub-plots of Figs. 19 and 20 from top to bottom show respectively the corresponding results of individual schemes.

As we can see from Fig. 19, the residuals of the first scheme ("non-corr") show systematic biases, and the

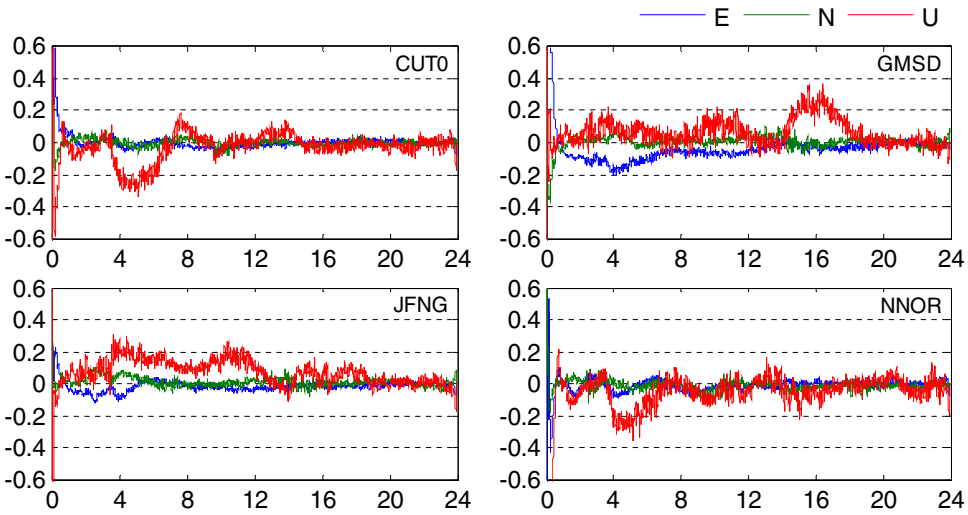


**Fig. 16** Positioning error (E:east/N:north/U:up) of B1B2 PPP. For each plot, the *horizontal axis* represents the universal time (unit: h), and the *vertical axis* represents the corresponding positioning error (unit: m)

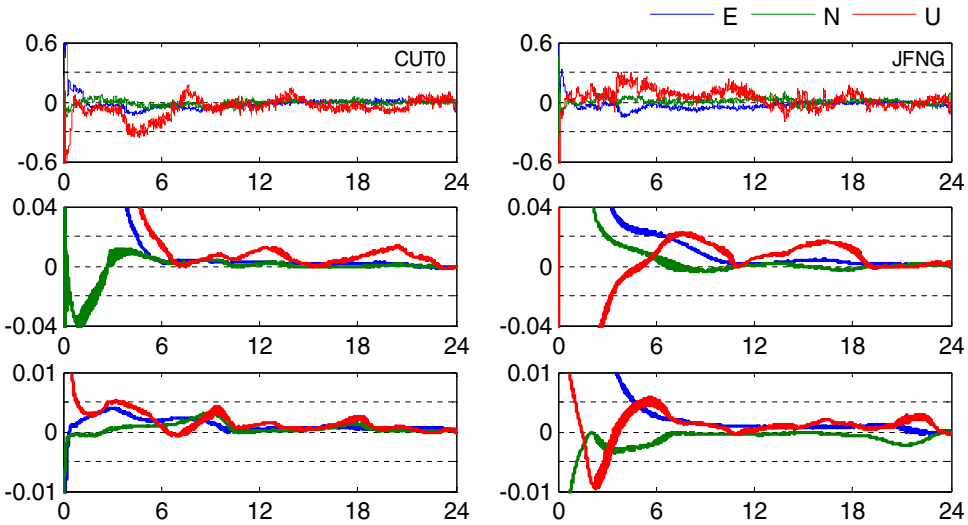


**Fig. 17** Positioning results (E:east/N:north/U:up) of B1B3 PPP. The *upper plots* show the positioning error of the third scheme ("dcb-corr"), while the *middle* and *lower plots* show the positioning differences with respect to the third scheme, using the first ("non-corr") and second ("tgd-corr") scheme, respectively. The *horizontal axis* represents the universal time (unit: h), and the *vertical axis* represents the position error or differences (unit: m)

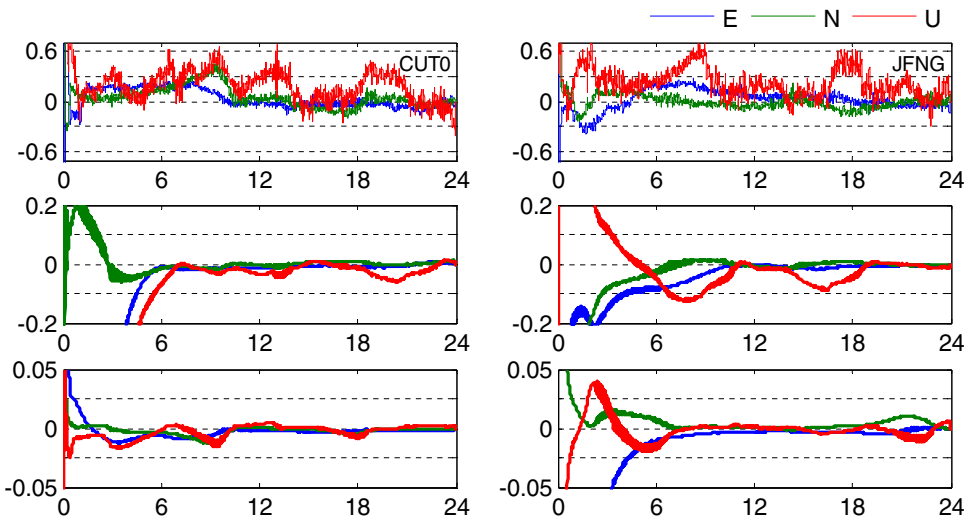


**Fig. 18** Positioning results (E:east/N:north/U:up) of B2B3 PPP. The *upper plots* show the positioning error of the third scheme ("dcb-corr"), while the *middle* and *lower plots* show the positioning differences with respect to the third scheme, using the first ("non-corr") and second ("tgd-corr") scheme, respectively. The *horizontal axis* represents the universal time (unit: h), and the *vertical axis* represents the position error or differences (unit: m)

**Table 5** Root mean squares of epoch-wise PPP solutions (unit: m)

| Mode | Scheme | CUT0 | | | GMSD | | | JFNG | | |
|---|---|---|---|---|---|---|---|---|---|---|
| | | E | N | U | E | N | U | E | N | U |
| B1B2 | non-corr | 0.018 | 0.021 | 0.088 | 0.047 | 0.025 | 0.081 | 0.021 | 0.025 | 0.072 |
| B1B3 | non-corr | 0.042 | 0.026 | 0.104 | 0.072 | 0.032 | 0.077 | 0.037 | 0.022 | 0.086 |
| | tgd-corr | 0.036 | 0.026 | 0.094 | 0.067 | 0.034 | 0.079 | 0.033 | 0.023 | 0.084 |
| | dcb-corr | 0.036 | 0.025 | 0.093 | 0.066 | 0.033 | 0.080 | 0.032 | 0.023 | 0.084 |
| B2B3 | non-corr | 0.144 | 0.138 | 0.192 | 0.158 | 0.097 | 0.207 | 0.101 | 0.083 | 0.183 |
| | tgd-corr | 0.108 | 0.133 | 0.163 | 0.140 | 0.079 | 0.190 | 0.085 | 0.065 | 0.159 |
| | dcb-corr | 0.105 | 0.130 | 0.162 | 0.139 | 0.081 | 0.191 | 0.086 | 0.067 | 0.159 |

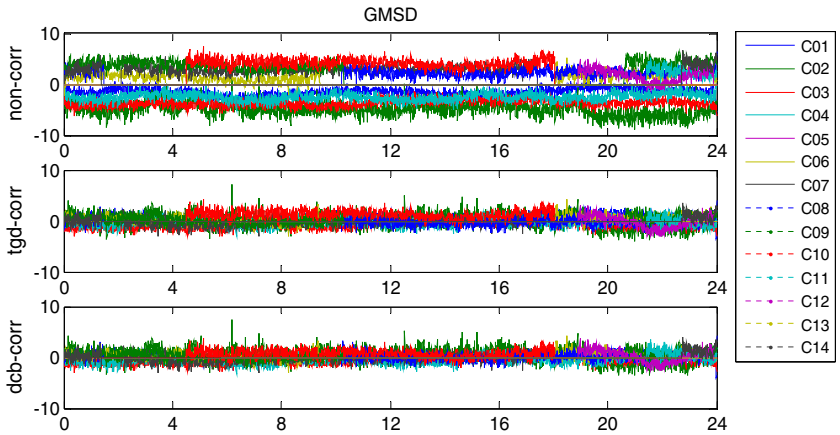


**Fig. 19** Pseudorange residuals: B1B3 PPP solutions on GMSD station. The *horizontal axis* represents the universal time (unit: h), and the *vertical axis* represents the pseudorange residuals (unit: m)

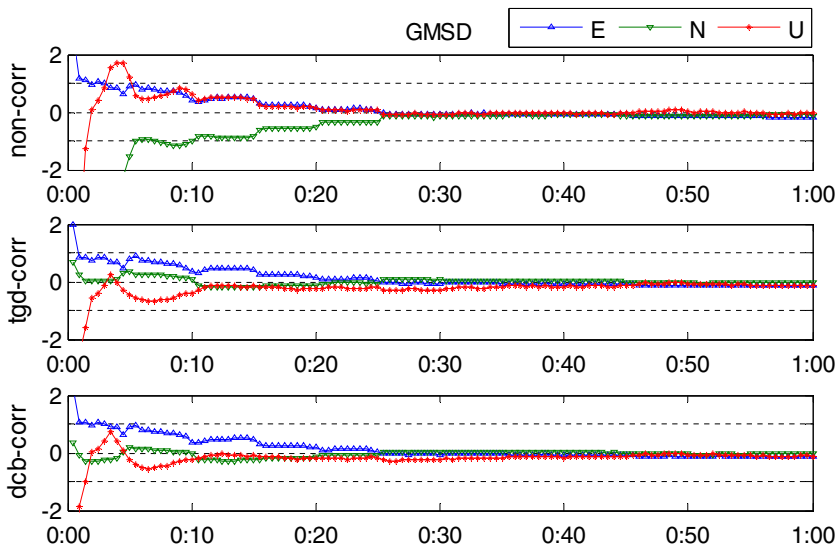


**Fig. 20** A case of PPP convergence: B1B3 PPP solutions on GMSD station. The *horizontal axis* represents the universal time (unit: h), and the *vertical axis* represents the positioning errors (unit: m)

satellite-dependent offsets range a few meters. In contrary, the residuals of the other two schemes ("tgd-corr" and "dcb-corr") look more reasonable, and run like zero-mean random noises. From the perspective of convergence, the positioning accuracy of the first 20–30 min is significantly degraded due to the uncorrected code biases. Tests using the B1B3 and B2B3 combinations on the other stations show the similar feature. But, it should be pointed out that, since the large amplification factor of B2B3 combination, the B2B3-based PPP is much more sensitive to the code biases. The residuals of the uncorrected pseudoranges reach tens of meters, and the positioning error may reach a few meters in the first 20 min.

To investigate the impact of differential code biases on the other parameters, Figs. 21, 22 and 23 show the differ-

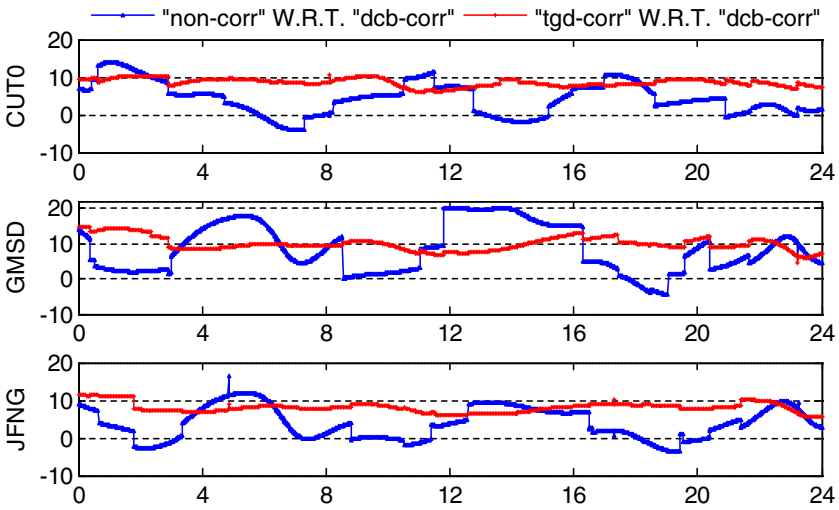


**Fig. 21** Differences of receiver clock bias estimates with respect to the third scheme ("dcb-corr"). The *horizontal axis* represents the universal time (unit: h), and the *vertical axis* represents the differences (unit: ns)

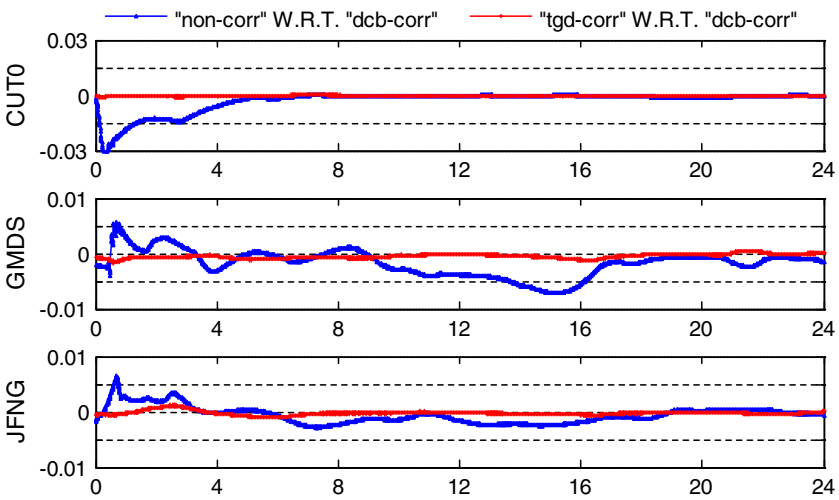


**Fig. 22** Differences of tropospheric delay estimates with respect to the third scheme ("dcb-corr"). The *horizontal axis* represents the universal time (unit: h), and the *vertical axis* represents the differences (unit: m)

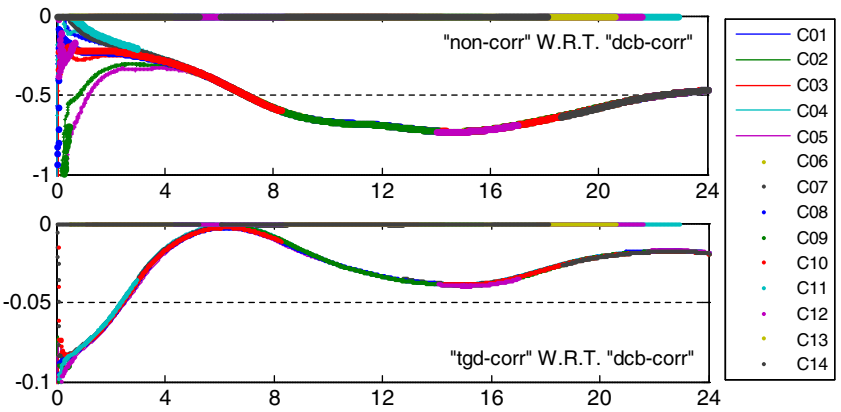


**Fig. 23** Differences of float ambiguity estimates with respect to the third scheme ("dcb-corr"). The *horizontal axis* represents the universal time (unit: h), and the *vertical axis* represents the differences (unit: m)

ences of the estimated receiver clock bias, tropospheric zenith path delay, and float ambiguities among the three different schemes based on the B1B3 PPP. The same feature can be observed in the B2B3 PPP with slightly larger differences, and will not be presented herein. As shown in Figs. 21, 22 and 23, all the other parameters in addition to the coordinates are subject to varying degrees of influences, depending on their correlations with the differential code biases. The unmodeled differential code biases are mostly absorbed into receiver clock estimates as well as the float ambiguities. The differences of receiver clock estimates range up to 10–20 ns with large variations over time if the differential code biases

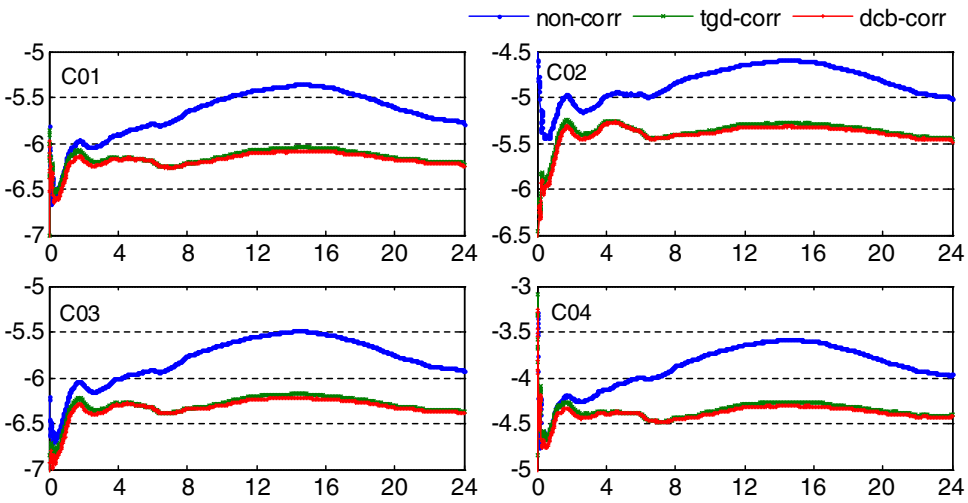


**Fig. 24** Float ambiguity estimates of a few GEO satellites. The *horizontal axis* represents the universal time (unit: h), and the *vertical axis* represents the ambiguities (unit: m)

are left uncorrected. Therefore, we should be very careful to take this issue into account while BDS is used for high-performance time and frequency transfer applications, such as precise timing. However, the clock differences between the latter two schemes, which utilize TGD and DCB parameters to account for the differential code biases, run much smoother and perform as a systematic bias of 9–10 ns for all stations. This is reasonable since a zero-mean average constraint has been introduced by the MGEX DCBs to solve the rank deficiency.

The tropospheric delay estimates are less sensitive to the differential code biases. In general, the tropospheric differences between the first and third scheme are within 5 mm after convergence, whereas the tropospheric estimates of the second and third schemes are almost the same value during the whole period. However, the float ambiguities are seriously affected by the differential code biases at the initial stage. Even worse, the influences on each satellite are different, and thus resulting in a much longer convergence time for the first scheme. Nevertheless, the differences in Fig. 23 show that the impacts of differential code biases are common to all satellites after convergence. In other words, the ambiguity differences of all satellites gradually converge to the same value at a specific epoch. In addition to the differences, the epoch-wise float ambiguities of a few GEO satellites are plotted in Fig. 24 to clearly show the importance of TGD/DCB corrections. The ambiguity estimates of the first scheme change over time with a large variation since part of the residual differential code biases is assimilated into the float ambiguities. However, the latter two schemes agree well with each other, and the estimated ambiguities run much smoother than the first scheme. One may notice that, the real estimates of ambiguities are not exactly constants after convergence even though the DCB corrections are applied. A variation of $\pm 0.1$ m is visible for the float ambiguities in the latter two schemes. This is mainly affected by the residual errors such as the uncalibrated phase delays (UPDs), antenna PCOs/PCVs and some other unmodeled errors. To separate the UPDs and to recover the integer nature of undifferenced ambiguities, the float ambiguities should be first conducted in wide lane (WL) and narrow lane (NL). Then the WL and NL UPDs are estimated from a reference network for use in further PPP ambiguity resolution. Therefore, such unstable float ambiguities will undoubtedly degrade the quality of UPD corrections and decrease the success rate of PPP integer ambiguity resolution.

## 5 Summary

This article first provides an overview of the currently available timing group delay (TGD) and differential code bias (DCB) parameters, and then reveals the relationship between TGDs and DCBs for BDS combining theoretical derivation and numerical experiments. Derivations shows that the meaning of BDS TGD is different from that of GPS, and the value of BDS TGD should be equal to the mean group delay differential. An indirect comparison indicates that the broadcast TGDs in navigation message agree well (within about 2 ns) with the MGEX DCBs after a zero-mean normalization. The cause of differential code bias is investigated, and the correction models for use in various occasions are developed for BDS positioning. TGD/DCB correction models for any single- (B1, B2, and B3) and dual-frequency (B1B2, B1B3, and B2B3) combinations from triple-frequency BDS signals are assessed by three different schemes, in which the differential code biases are either ignored, or corrected with TGD or DCB parameters.

Comparative analysis of the influence of differential code biases on BDS positioning reveal that, the uncorrected code biases seriously degrade the positioning accuracy of (B1, B2 single-frequency, B1B2, B1B3 and B2B3 dual-frequency)

SPP, whereas the (B1B3 and B2B3 dual-frequency) PPP estimates are subject to varying degrees of influences, depending on their correlations with the differential code biases. Both the broadcast TGD and MGEX DCB parameters are benefit for the performance of BDS positioning, and the SPP/PPP solutions corrected by TGDs and DCBs agree well with each other, which further confirm their equivalence. Even though the impacts of differential code biases on PPP are smoothed over time, it is unwise to ignore the differential code biases since the biases will be partly absorbed by other estimates such as receiver clock bias, tropospheric delay and carrier phase ambiguities. Consequently, the bias-contaminated float ambiguities would increase the PPP convergence time and decrease the success rate of zero-differenced ambiguity resolution. Therefore, for the high-performance positioning and timing applications, it is essential to adopt a proper TGD or DCB correction model for BDS.

**Acknowledgments** The authors gratefully acknowledge IGS Multi-GNSS Experiment (MGEX) for providing GNSS data and products. We also appreciate the editor-in-chief, Roland Klees, the handling editor, Pascal Willis, and three anonymous reviewers for their valuable comments and improvements to this manuscript. This study was supported by the National Natural Science Foundation of China (No: 41474025, No: 41404006) and International Postdoctoral Exchange Fellowship Program 2013 by the Office of China Postdoctoral Council (No. 2013042).

## References

Abdel-salam M (2005) Precise point positioning using un-differenced code and carrier phase observations. Dissertation, University of Calgary, Canada. UCGE reports no. 20229

CSNO (2012) BeiDou navigation satellite system signal in space interface control document-open service signal B1I, version 1.0. China Satellite Navigation Office, Dec 2012

CSNO (2013) BeiDou navigation satellite system signal in space interface control document-open service signal, version 2.0. China Satellite Navigation Office, Dec 2013

Dach R, Montenbruck O, Prange L (2014) Status of the IGS-MGEX project. In: Proceedings of EUREF 2014 symposium, Vilnius, Lithuania, 3–7 June

Deng Z, Zhao Q, Springer T, Prange L, Uhlemann M (2014) Orbit and clock determination-BeiDou. In: Proceedings of IGS workshop, Pasadena, USA, 23–27 June

Dow JM, Neilan RE, Rizos C (2009) The International GNSS Service in a changing landscape of global navigation satellite systems. J Geod 83(7):191–198. doi:10.1007/s00190-008-0300-3

Feltens J, Schaer S (1998) IGS products for the ionosphere, IGS positioning paper. In: Proceedings of the IGS analysis centers workshop, Darmstadt, Germany, 9–11 Feb

Gao Y (2008) GNSS biases, their effect and calibration. In: Proceedings of IGS workshop, Miami Beach, USA, 2–6 June

He L, Ge M, Wang J, Wickert J, Schuh H (2013) Experimental study on the precise orbit determination of the BeiDou navigation satellite system. Sensors 13(3):2911–2928. doi:10.3390/s130302911

Hernández-Pajares M, Juan J, Sanz J, Orus R, Garcia-Rigo A, Feltens J, Komjathy A, Schaer S, Krankowski A (2009) The IGS VTEC maps: a reliable source of ionospheric information since 1998. J Geod 83(3):263–275. doi:10.1007/s00190-008-0266-1

Kouba J, Hérous P (2001) Precise point positioning using IGS orbit and clock products. GPS Solut 5(2):12–28. doi:10.1007/PL00012883

Li M, Qu L, Zhao Q, Guo J, Su X, Li X (2014) Precise point positioning with the BeiDou navigation satellite system. Sensors 14(1):927–943. doi:10.3390/s140100927

Li Z, Yuan Y, Li H, Ou J, Huo X (2012) Two-step method for the determination of the differential code biases of COMPASS satellites. J Geod 86(11):1059–1076. doi:10.1007/s00190-012-0565-4

Liu J, Bi S, Zheng J, Xie J (2014) Effect of separation of navigation satellite antenna inter-frequency phase centers on TGD parameter. In: China satellite navigation conference (CSNC) 2014 Proceedings. Lecture notes in electrical engineering, vols II, 304, pp 227–238. doi:10.1007/978-3-642-54743-0_20

Lou Y, Liu Y, Shi C, Yao X, Zheng F (2014) Precise orbit determination of BeiDou constellation based on BETS and MGEX network. Sci Rep 4:4692. doi:10.1038/srep04692

Montenbruck O, Steigenberger P (2013) The BeiDou navigation message. J Glob Position Syst 12(1):1–12. doi:10.5081/jgps.12.1.1

Montenbruck O, Hauschild A, Steigenberger P, Hugentobler U, Teunissen P, Nakamura S (2013) Initial assessment of the COMPASS/BeiDou-2 regional navigation satellite system. GPS Solut 17(2):211–222. doi:10.1007/s10291-012-0272-x

Montenbruck O, Steigenberger P, Hauschild A (2014) Differential code bias estimation using multi-gnss observations and global ionosphere maps. In: Proceedings of ION ITM 2014, San Diego, USA, 26–28 Jan

Petit G, Luzum B (2010) IERS Conventions 2010 (IERS Technical Note No. 36). Verlag des Bundesamts für Kartographie und Geodäsie, Frankfurt am Main, p 179. ISBN:3-89888-989-6.

Rao GS (2007) GPS satellite and receiver instrumental biases estimation using least squares method for accurate ionosphere modeling. J Earth Syst Sci 116:407–411. doi:10.1007/s12040-007-0039-x

Ray J (2001) Updated P1–C1 biases and cc2noncc. IGS Mail No. 3220, 5 March

Rizos C, Montenbruck O, Weber R, Neilan R, Hugentobler U (2013) The IGS MGEX Experiment as a milestone for a comprehensive multi-GNSS service. In: Proceedings of ION-PNT-2013, Honolulu, USA, 22–25 April

Schaer S (2003) IGS GLONASS tracking data. IGS Mail No. 4371, 8 May.

Schaer S (2008) Differential code biases (DCB) in GNSS analysis. In: Proceedings of IGS workshop, Miami Beach, USA, 2–6 June

Schaer S (2012) Overview of relevant GNSS biases. In: Proceedings of IGS workshop on GNSS biases. University of Bern, Switzerland, 18–19 Jan

Schaer S, Steigenberger P (2006) Determination and use of GPS differential code biases values. In: Proceedings of IGS workshop, Darmstadt, Germany, 8–11 May

Shi C, Zhao Q, Hu Z, Liu J (2013) Precise relative positioning using real tracking data from COMPASS GEO and IGSO satellites. GPS Solut 17(1):103–119. doi:10.1007/s10291-012-0264-x

Tetewsky A, Ross J, Soltz A, Vaughn N, Anzperger J, O'Brien C, Graham D, Craig D and Lozow J (2009) Making sense of inter-signal corrections-accounting for GPS satellite calibration parameters in legacy and modernized ionosphere correction algorithms. InsideGNSS:37–48, July/August

Wu JT, Wu SC, Hajj GA, Bertiger WI, Lichten SM (1993) Effects of antenna orientation on GPS carrier phases. Man Geod 18:91–98

Wu X, Hu X, Wang G, Zhong H, Tang C (2013) Evaluation of COMPASS ionospheric model in GNSS positioning. Adv Space Res 51(6):959–968. doi:10.1016/j.asr.2012.09.039

Yang YX, Li JL, Wang AB, Xu JY, He HB, Guo HR, Shen JF, Dai X (2014) Preliminary assessment of the navigation and positioning

performance of BeiDou regional navigation satellite system. Sci China Earth Sci 57(1):144–152. doi:10.1007/s11430-013-4769-0

Zhang X, Liu J, Forsberg R (2006) Application of precise point positioning in airborne survey. Geomat Inform Sci Wuhan Univ 31(1):19–22 (in Chinese)

Zhao Q, Guo J, Li M, Qu L, Hu Z, Shi C, Liu J (2013) Initial results of precise orbit and clock determination for COMPASS navigation satellite system. J Geod 87(5):475–486. doi:10.1007/s00190-013-0622-7